Fast phase reconstruction from phase differences using sub-aperture stitching method

Jun Wu (吴 峻)[1*] and Jiancheng Xu (徐建程)[2]

[1]*Network Center of Zhejiang Medical College, Hangzhou 310053, China*

[2]*Institute of Information Optics, Zhejiang Normal University, Jinhua 321004, China*

[*]*Corresponding author: wjybbbbbb@126.com*

Received August 30, 2012; accepted November 16, 2012; posted online December 29, 2012

A wavefront reconstruction algorithm based on sub-aperture stitching is proposed to reconstruct a phase from its phase differences to improve calculation efficiency. The proposed algorithm is similar to the sub-aperture stitching interferometry. It divides large phase grids into several small sub-apertures, reconstructs the phase of each sub-aperture from the phase differences through the standard wavefront reconstruction algorithm, and then stitches the results of the sub-apertures together. The proposed algorithm can efficiently reconstruct the phase with much less computer memory and calculation time. Simulations and experiments are conducted to demonstrate the effectiveness of the proposed algorithm.

OCIS codes: 120.3180, 120.6650, 120.4800.

doi: 10.3788/COL201210.S21202.

The wavefront reconstruction algorithm in lateral shearing interferometry is a typical inverse procedure that reconstructs wavefront from its phase differences, and thus critical for wavefront measurement. Several algorithms[1−13] have been investigated and proposed. Among these algorithms, 1) integration methods are direct, simple, and rapid reconstruction algorithms. However, these methods suffer from several disadvantages, such as noise accumulation, error propagation, and restricted measurement area[1−2]; 2) Polynomial fitting methods[3−4] can reduce noise accumulation and have good error propagation properties. However, prior knowledge of the test surface is necessary to ensure good accordance of the selected polynomial with the test surface; 3) Fourier transformation methods[5−6] require hardly any preconditions of the test surface and need less computational effort. However, the information of shear periodic parts in such algorithms can be lost[5]; 4) Partial differential equation (PDE) methods[7−13] require no prior knowledge of the wavefront and have no noise accumulation. However, these methods need a very large computational effort to solve a set of equations. Several studies have attempted to solve such set of equations by iterative numerical schemes[8−9]. However, the convergence rate is slow when the phase grid is large[12]. Hence, PDE methods require a large computer memory and calculation time, thereby decreasing phase efficiency. The resolution of commercial interferometer in lateral shearing interferometry is more than 240×320. Therefore, the size of the coefficient matrix[7−8] that connects the phase and its differences is larger than $2\times(240\times320)^2$. This size is significantly large that the existing PDE methods[7−13] fail to reconstruct the phase efficiently.

A new wavefront reconstruction algorithm based on sub-aperture stitching was proposed in this study to improve the calculation efficiency. This new algorithm is similar to the sub-aperture stitching interferometry[14,15]. In this algorithm the large phase grid was divided into several small sub-apertures; the phase of each sub-aperture was reconstructed from phase differences by the Hudgin wavefront sensor geometry[7]; and the results of sub-apertures were stitched together. The proposed algorithm can efficiently reconstruct the phase with much less computer memory and calculation time. In addition, it has potential application in lateral shearing interferometry, especially for the reconstruction of large phase grid. Firstly, the principle of the proposed algorithm is discussed, and then its effectiveness is verified by computer simulation and experiment.

In a standard Fizeau interferometer, the measured phase of the test surface is obtained and expressed as

$$\Phi^0(x,y) = \phi(x,y) - \phi_{\rm R}(x,y), \tag{1}$$

where $\phi(x,y)$ and $\phi_{\rm R}(x,y)$ represent the true phases of the test and reference beams, respectively. The test surface was laterally shifted along x and y axes and the shifting amounts were approximated to the transverse spatial resolution of the interferometer[11]. Two new phase maps were obtained and expressed as

$$\Phi^x(x,y) = \phi(x+1,y) - \phi_{\rm R}(x,y), \tag{2}$$

$$\Phi^y(x,y) = \phi(x,y+1) - \phi_{\rm R}(x,y). \tag{3}$$

According to the three measured phase maps, Φ^0, Φ^x, and Φ^y, the absolute phase differences of the test surface between the nearest X- and Y-neighbor spatial cells on the test surface can be obtained as

$$\begin{aligned}\phi^x(x,y) &= \phi(x+1,y) - \phi(x,y)\\ &= \Phi^x(x,y) - \Phi^0(x,y),\end{aligned} \tag{4}$$

$$\begin{aligned}\phi^y(x,y) &= \phi(x,y+1) - \phi(x,y)\\ &= \Phi^y(x,y) - \Phi^0(x,y),\end{aligned} \tag{5}$$

where $\phi^x(x,y)$ and $\phi^y(x,y)$ represent the absolute phase differences of $\phi(x,y)$, which correspond to the partial derivatives of the true phase of the test surface. The absolute phase measurement of the test surface can be performed by virtual lateral shearing interferometry by reconstructing the true phase $\phi(x,y)$ from $\phi^x(x,y)$ and $\phi^y(x,y)$[16].

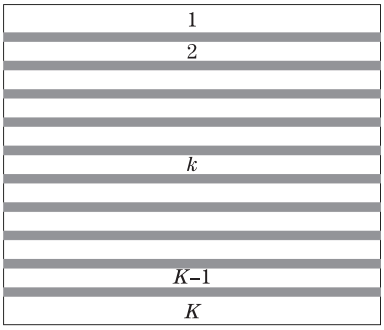

Fig. 1. Schematic of the division of the large phase into several small sub-apertures.

Assume that the phase of the test surface is expressed discretely as an array $\phi_{i,j}$, i=1, 2, $\cdots$, L; j=1, 2, $\cdots$, M, where L and M denote the size numbers of the matrix ϕ in the row and column directions, respectively. The large phase array ϕ is then divided into K small sub-apertures, as shown in Fig. 1. The phase array in each sub-aperture has N rows and M columns and is expressed as $\phi^k_{i,j}$, where i=1, 2, $\cdots$, N; j=1, 2, $\cdots$, M; k=1, 2, $\cdots$, K. Herein, N is far less than L, (i.e., $N \ll L$). For $1< k < K$, the kth sub-aperture has to overlap with the (k–1)th and (k+1)th sub-apertures, as shown in Fig. 1. The overlap region has P rows and Mcolumns, where $1\leqslant P<N$. Through the geometric analysis of Fig. 1, the relation of N, P, K, and L was obtained and expressed as

$$L = KN - (K-1)P. \tag{6}$$

The phase array in the kth sub-aperture has N rows and M columns, which can be reconstructed from the absolute phase differences $\phi^x(x,y)$ and $\phi^y(x,y)$. The discrete version of phase differences can be expressed as

$$\phi^x_{i,j} = \phi_{i,j+1} - \phi_{i,j}, (1 \leqslant i \leqslant N,\ 1 \leqslant j \leqslant M-1); \tag{7}$$

$$\phi^y_{i,j} = \phi_{i+1,j} - \phi_{i,j}, (1 \leqslant i \leqslant N-1,\ 1 \leqslant j \leqslant M). \tag{8}$$

According to Eqs. 7 and 8, the relation between the phase and the phase differences can be rewritten as

$$\Delta\varphi = A\varphi, \tag{9}$$

where $\Delta\varphi$ and φ are one-dimensional (1D) arrays, and $\varphi = [\phi_{1,1}K\phi_{1,M}K\phi_{2,1}K\phi_{2,M}K\phi_{N,1}K\phi_{N,M}]^{\mathrm{T}}$ and $\Delta\varphi = [\phi^x_{1,1}K\phi^x_{1,M-1}\phi^x_{2,1}K\phi^x_{2,M-1}K\phi^x_{N,1}K\phi^x_{N,M-1}\phi^y_{1,1}K\phi^y_{1,M}$ $\phi^y_{2,1}K\phi^y_{2,M}K\phi^y_{N-1,1}K\phi^y_{N-1,M}]^{\mathrm{T}}$. The lengths of $\Delta\varphi$ and φ are $2MN-M-N$ and MN, respectively. The matrix of A that relates the arrays $\Delta\varphi$ and φ can be expressed as

$$A = \begin{bmatrix} D \\ E \end{bmatrix}, \tag{10}$$

where D and E can be expressed as

$$D = \begin{bmatrix} D_1 & & & & \\ & D_2 & & & \\ & & D_3 & & \\ & & & O & \\ & & & & D_N \end{bmatrix}, \tag{11}$$

where

$$D_1 = D_2 = D_3 = K = D_N = \begin{bmatrix} -1 & 1 & & & & \\ & -1 & 1 & & & \\ & & -1 & 1 & & \\ & & & K & & \\ & & & & -1 & 1 \end{bmatrix}, \tag{12}$$

and

$$E = \begin{bmatrix} -1 & & 1 & & & \\ & -1 & & 1 & & \\ & & -1 & & 1 & \\ & & & K & & \\ & & & & -1 & 1 \end{bmatrix}, \tag{13}$$

where D_N, D, and E are the relations between φ and the nth row of $\phi^x(x,y)$, $\phi^x(x,y)$, and $\phi^y(x,y)$, respectively. D is a diagonal matrix containing D_N and every row of E between –1 and 1 comprises M–1 zeros. The sizes D_N, D, and E are $(M-1)\times M$, $N(M-1)\times MN$, and $M(N-1)\times MN$, respectively, thus the size of A is $(2MN-M-N)\times MN$.

Herrmann[10] indicated that using the zero-mean condition leads to an extended A_{e} matrix that meets the condition where $A^{\mathrm{T}}_{\mathrm{e}}A_{\mathrm{e}}$ is not singular. The extended A_{e} and $\Delta\varphi_{\mathrm{e}}$ are expressed as

$$A_{\mathrm{e}} = \begin{bmatrix} A \\ F \end{bmatrix}, \tag{14}$$

and

$$\Delta\varphi_{\mathrm{e}} = \begin{bmatrix} \Delta\varphi \\ Z \end{bmatrix}, \tag{15}$$

where F is a matrix consisting entirely of ones and Z is a matrix consisting entirely of zeros. The sizes of F and Z are $(M+N)\times MN$ and $(M+N)\times 1$, respectively. Thus, the sizes of A_{e} and $\Delta\varphi_{\mathrm{e}}$ become $2MN\times MN$ and $2MN\times 1$, respectively. Finally, the phase in the sub-aperture can be reconstructed as[8,10]

$$\varphi = (A^{\mathrm{T}}_{\mathrm{e}}A_{\mathrm{e}})^{-1}A^{\mathrm{T}}_{\mathrm{e}}\Delta\varphi_{\mathrm{e}}. \tag{16}$$

The two-dimensional (2D) phase array ϕ can be easily obtained from the 1D phase array φ.

The calculation of Eq. (16) leads to a consumption of large computer memory and calculation time because the extended matrix A_{e} is a big sparse matrix[8,10]. The computer memory needed in the calculation increases fast with the square of MN. However, in our proposed algorithm, the phase array was divided into several small sub-apertures to ensure that N is a small number ($N \ll L$) to effectively reduce the computer memory needed. In addition, the big phase array was divided into sub-apertures with equal sizes. Thus, $(A^{\mathrm{T}}_{\mathrm{e}}A_{\mathrm{e}})^{-1}A^{\mathrm{T}}_{\mathrm{e}}$ remains constant for all sub-apertures and is calculated only once, which effectively reduces the calculation time needed.

After the phase array ϕ in each sub-aperture is reconstructed, the results of sub-apertures are stitched together. The obtained phase array ϕ in each sub-aperture has zero mean, which is not true in most cases. If the results are simply stitched according to the spatial position of the sub-aperture without compensating the mean of the phase in each sub-aperture, a phase step error

will result in the final stitched phase map, as shown in Fig. 2(a). Figure 2(b) shows the 1D phase error of Fig. 2(a), wherein a phase step error between the adjacent sub-apertures in row direction of the phase array is observed. However, the phase step error can be compensated by

$$\phi_{k+1}^{\mathrm{C}} = \phi_{k+1} + \mathrm{mean}[\phi_k(x_{k,k+1})] - \mathrm{mean}[\phi_{k+1}(x_{k,k+1})],\ (k = 1 : K-1), \quad (17)$$

where ϕ_{k+1}^{C} represents the compensated phase, ϕ_k and ϕ_{k+1} represent the phase array before comensation in the kth and the $(k+1)$th sub-apertures, respectively. The operators $\mathrm{mean}[\phi_k(x_{k,k+1})]$ and $\mathrm{mean}[\phi_{k+1}(x_{k,k+1})]$ represent the averages of the phases ϕ_k and ϕ_{k+1} in the overlap between the kth and the $(k+1)$th sub-apertures, respectively, wherein the overlap has P rows and M columns. Finally, the compensated phase is stitched together according to the spatial position of the sub-aperture. The stitched phase is shown in Fig. 3(a); its phase error in the row direction is shown in Fig. 3(b). The phase step error was effectively reduced by compensating the mean of the phase in each sub-aperture according to Eq. (17), as shown in Fig. 3. The residual phase error in Fig. 3(b) was mainly caused by the random noise in the phase differences.

The exact expression of an actual object surface is hard to determine because of several practical factors. Thus, a series of computer simulations were carried out to verify the effectiveness of the proposed algorithm. We assume that the given measured phase is ϕ=peaks(601), where peaks is a sample function of two variables in Matlab. The given phase has 601 rows and 601 columns (i.e., $L = M = 601$), as shown in Fig. 4(a). The phase differences ϕ^x and ϕ^y were calculated using Eqs. (4) and (5). In addition, the phase differences were added by a normal random noise (mean = 0 and standard deviation = 0.001). The signal-to-noise ratio (SNR) of the phase difference was about 14.07 dB. SNR was defined as the ratio of the standard deviation of the calculated phase differences to that of the random noise. The noised phase differences in the column and row directions are shown in Figs. 4(b) and (c), respectively.

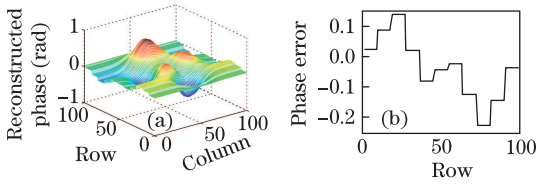

Fig. 2. (a) Stitched phase without compensation of the mean of phase in each sub-aperture and (b) 1D phase error of (a) in the row direction.

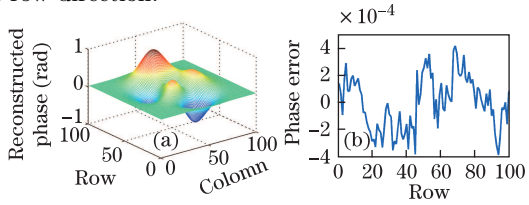

Fig. 3. (a) Stitched phase with compensation of the mean of phase in each sub-aperture and (b) 1D phase error of (a) in the row direction.

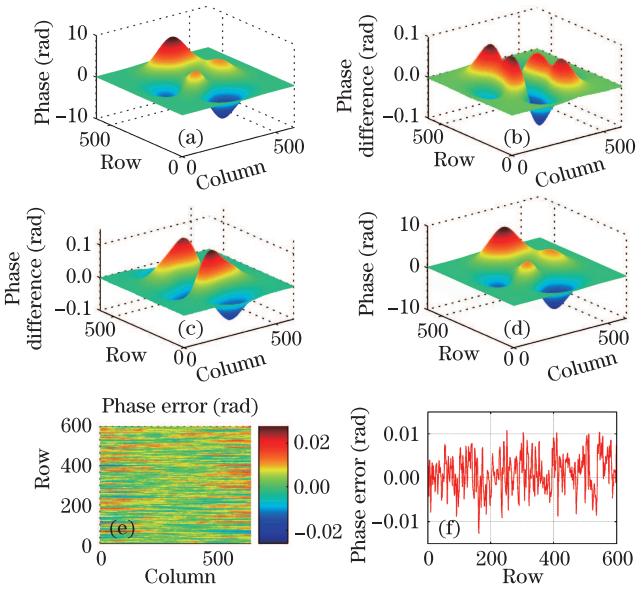

Fig. 4. Simulation results. (a) The given phase, (b) and (c) the phase differences in the column and row directions, respectively, (d) the reconstructed phase, (e) the reconstructed phase error, and (f) one-dimensional phase error in the 300 th column.

The given phase was divided into 300 sub-apertures by setting N=3 and P=1. The proposed algorithm was then applied, and the phase was reconstructed and stitched. Figure 4(d) shows the final reconstructed phase from Figs. 4(b) and (c). The reconstructed phase error of the proposed algorithm was obtained by comparing the reconstructed phase with the given phase, as shown in Fig. 4(e). The peak-to-valley and root-mean-square (RMS) values of Fig. 4(e) were 0.0545 and 0.0061 rad, respectively. Figure 4(f) shows the 1D phase error of Fig. 4(e) in the 300th column. The proposed algorithm exhibited random reconstructed phase error, which is mainly caused by the added random noise in the phase differences. The simulation showed that the proposed algorithm can effectively reconstruct the phase from phase differences even if the phase grid is very large.

The aforementioned simulation was processed with a 2.6-GHz laptop using MATLAB. The total processing time was about 39 s under the setting of N=3, P=1, and M=601. However, if the phase from phase differences is directly reconstructed using Eq. (16) by setting $M = N$=601, it will fail to calculate because it is out of the computer memory. We assume that the given phase has a size of 61×61, i.e., $L = M$=61, the processing time of the Hudgin's reconstruction method[7] ($N = M$=61) is 144.875 s, and the processing time of the reconstruction method (N=3 and M=61) is 0.078 s to show the calculation efficiency of the proposed algorithm. The division of the large phase grid into several small sub-apertures can effectively reduce the processing time of wavefront reconstruction. Based on the simulation results, we conclude that the proposed algorithm can reduce the calculation time and computer memory needed.

The accuracy of the proposed algorithm depends on the SNR of the phase differences. Thus, we reconstructed

the phase using the proposed algorithm from the phase differences with different SNRs and obtained the RMS values of the reconstructed phase error, as shown in Fig. 5. The reconstructed phase error of the proposed algorithm decreases with increasing SNR of the phase differences.

The proposed algorithm was used for virtual lateral shearing interferometry to further verify its performance. The measurement of a flat was performed in a sub-aperture stitching interferometer (SSI) developed by QED. The test flat was measured 50 times in the original position, and the average of the measurement was calculated and shown in Fig. 6(a). Figures 6(b) and (c) show the phase differences in the column and row directions calculated from Fig. 6(a) by digital differential. The phase was then reconstructed from Figs. 6(b) and (c), and shown in Fig. 6(d). Figure 6(d) agrees well with Fig. 6(a), thereby demonstrating the effectiveness of the proposed algorithm in reconstructing phase from the phase differences. The reconstructed phase contains

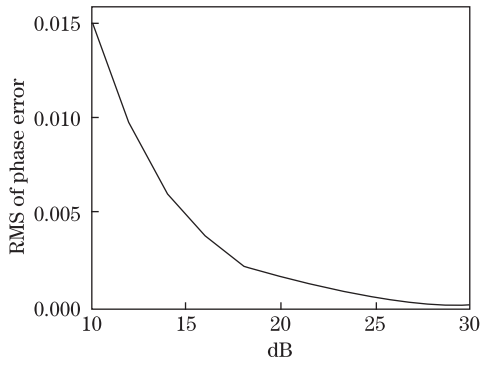

Fig. 5. Relation between the constructed phase error and the SNR of the phase differences.

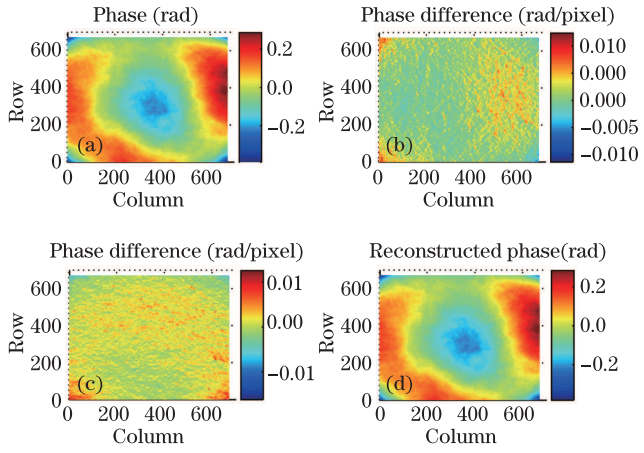

Fig. 6. Experiment of phase reconstruction. (a) The measured phase (b) and (c) the calculated phase differences of (a) in column and row directions, and (d) the reconstructed phase from (b) and (c).

the phase of the reference surface in the SSI because the phase differences were calculated from Fig. 6(a), as shown in Fig. 6(d).

In conclusion, the wavefront reconstruction algorithm, which reconstructs the phase from its phase differences, is critical for lateral shearing interferometry and virtual lateral shearing interferometry. In this study, a wavefront reconstruction algorithm with high calculation efficiency is proposed based on sub-aperture stitching. The proposed algorithm divides large phase grids into several small sub-apertures, reconstructs the phase of each sub-aperture from phase differences by the standard wavefront reconstruction algorithm, and stitches the results of sub-apertures together. Simulations and experiments are carried out to demonstrate the effectiveness of the proposed algorithm. The simulations show that the division of the large phase grid into several small sub-apertures with equal size effectively reduced the calculation time and computer memory needed. The processing time of the proposed algorithm is about 39 s when the phase grid was 601×601. In addition, the reconstructed phase error of the proposed algorithm decreased with increasing SNR of the phase differences. The experiment shows that the proposed algorithm can be applied to virtual lateral shearing interferometry.

This work was supported by the Natural Science Foundation of Zhejiang Province of China under Grant No. Y1110125.

References

1. S. Okuda, T. Nomura, K. Kamiya, H. Miyashiro, K. Yoshikawa, and H. Tashiro, Appl. Opt. **39,** 5179 (2000).
2. X. Tian, M. Itoh, and T. Yatagai, Appl. Opt. **34,** 7213 (1995).
3. G. Harbers, P. J. Kunst, and G. W. R. Leibbrandt, Appl. Opt. **35,** 6162 (1996).
4. H. Brug, Appl. Opt. **36,** 2788 (1997).
5. C. Elster and I. Weingärtner, Appl. Opt. **38,** 5024 (1999).
6. A. Dubra, C. Paterson, and C. Dainty, Appl. Opt. **43,** 1108 (2004).
7. R. H. Hudgin, J. Opt. Soc. Am. **67,** 375 (1977).
8. B. R. Hunt, J. Opt. Soc. Am. **69,** 393 (1979).
9. W. H. Southwell, J. Opt. Soc. Am. **70,** 998 (1980).
10. J. Herrmann, J. Opt. Soc. Am. **70,** 28 (1980).
11. H. Takajo and T. Takahashi, J. Opt. Soc. Am. **5,** 416 (1988).
12. D. C. Ghiglia and L. A. Romero, Opt. Lett. **14,** 1107 (1989).
13. P. Liang, J. Ding, Z. Jin, C. Guo, and H. Wang, Opt. Express **14,** 625 (2006).
14. M. Bray, Proc. SPIE **3134,** 39 (1997).
15. P. Murphy, J. Fleig, and G. Forbes, Proc. SPIE **6293,** 62930J1 (2006).
16. E. E. Bloemhof, Opt. Lett. **35,** 2346 (2010).